Chemical Science

ROYAL SOCIETY OF CHEMISTRY

EDGE ARTICLE

View Article Online
View Journal | View Issue

Check for updates

Cite this: *Chem. Sci.*, 2025, **16**, 10742

All publication charges for this article have been paid for by the Royal Society of Chemistry

Received 27th March 2025
Accepted 11th May 2025

DOI: 10.1039/d5sc02334c

rsc.li/chemical-science

Rational design of circularly polarized luminescence active chiral metal–organic frameworks for logic devices†

Hongrui Zheng, Qingqing Wang, Fei Wang,* Shangda Li* and Jian Zhang*

Chiral metal–organic frameworks (CMOFs) have garnered significant attention for their remarkable potential in circularly polarized luminescence (CPL) applications. This study employs circularly polarized fluorescence energy transfer (CPF-ET) as a pivotal strategy for engineering CPL-active CMOFs. Three pairs of structurally analogous CMOFs (**L/D-1**, **L/D-2**, and **L/D-3**) were synthesized by coupling homochiral imidazolium dicarboxylates (L/D-H_2IDPA) with terephthalic acid (TPA) derivatives. These CMOFs displayed distinctive fluorescence and persistent afterglow phosphorescence. As anticipated, these compounds demonstrated outstanding CPL performances, with $|g_{lum}|$ values reaching up to 0.55 in their single-crystal form. Mechanistic studies revealed a strong correlation between the asymmetry factor and CPF-ET efficiency. These extraordinary CPL properties were leveraged for groundbreaking applications, such as chiral logic devices for sophisticated information encryption. This work lays a robust theoretical and practical foundation for advancing CPL-active materials and seamlessly integrating them into state-of-the-art optoelectronic technologies.

Introduction

Circularly polarized luminescence (CPL) refers to the emission of circularly polarized light from an excited chiral luminescent system, characterized by pronounced differences in polarization between left- and right-handed circularly polarized states.[1–3] Materials exhibiting CPL characteristics have shown considerable promise for a broad range of applications, including anti-counterfeiting, 3D imaging, and optical data storage.[4–7] Recently, circularly polarized fluorescence energy transfer (CPF-ET), an advanced extension of Förster resonance energy transfer (FRET), has emerged as a novel mechanism that integrates the chirality transfer with energy transfer processes, providing enhanced insights into the generation and amplification of CPL signals.[8–12] Within this system, a critical factor influencing CPL is the degree of energetic compatibility between the donor and acceptor.[13–15] Specifically, when the emission spectrum of the chiral moiety (donor) overlaps with the absorption (or excitation) spectrum of the luminescent moiety (acceptor), the CPL phenomenon can be initiated through the CPF-ET process in the overlapping spectral region (Scheme 1a).[16–18] Furthermore, the extent of spectral overlap exhibits a direct, positive correlation with CPL efficiency. As a result, CPF-ET provides a robust foundation for the rational design and synthesis of CPL-active materials.

Chiral metal–organic frameworks (CMOFs) represent a class of chiral crystalline materials characterized by a periodic network structure, wherein metal ions or clusters are coordinated with organic ligands through self-assembly.[19–21] These materials exhibit exceptional structural tunability and design flexibility, making them highly promising for CPL.[22,23] Among the various methods for constructing CPL-active CMOFs, a straightforward approach involves the dual-ligand strategy, where two independent ligands—one imparting chirality and the other exhibiting luminescent property—are simultaneously integrated into a single MOF structure.[24–27] Furthermore, prior to the assembly process, CPF-ET can be utilized to predict the potential CPL performance of various ligand combinations, thereby minimizing the trial-and-error nature of the experimental design. Homochiral imidazolium dicarboxylates, such as L/D-H_2IDPA, represent an innovative class of chiral ligands with considerable potential for constructing functional CMOFs and are actively being investigated in our laboratory.[28,29] Additionally, terephthalic acid (TPA) and its derivatives, as easily accessible aromatic ligands exhibiting excellent luminescent properties are extensively employed in the construction of luminescent MOFs.[30–32] Based on the principles of CPF-ET, we analyzed the compatibility between the emission spectrum of L/D-H_2IDPA and the absorption spectrum of TPA. Notably, a significant overlap between these spectra was observed, which

---

State Key Laboratory of Structural Chemistry, Fujian Institute of Research on the Structure of Matter, The Chinese Academy of Sciences, Fuzhou, Fujian 350002, People's Republic of China. E-mail: wangfei04@fjirsm.ac.cn; sdli@fjirsm.ac.cn; zhj@fjirsm.ac.cn

† Electronic supplementary information (ESI) available. CCDC 2415207–2415212. For ESI and crystallographic data in CIF or other electronic format see DOI: https://doi.org/10.1039/d5sc02334c

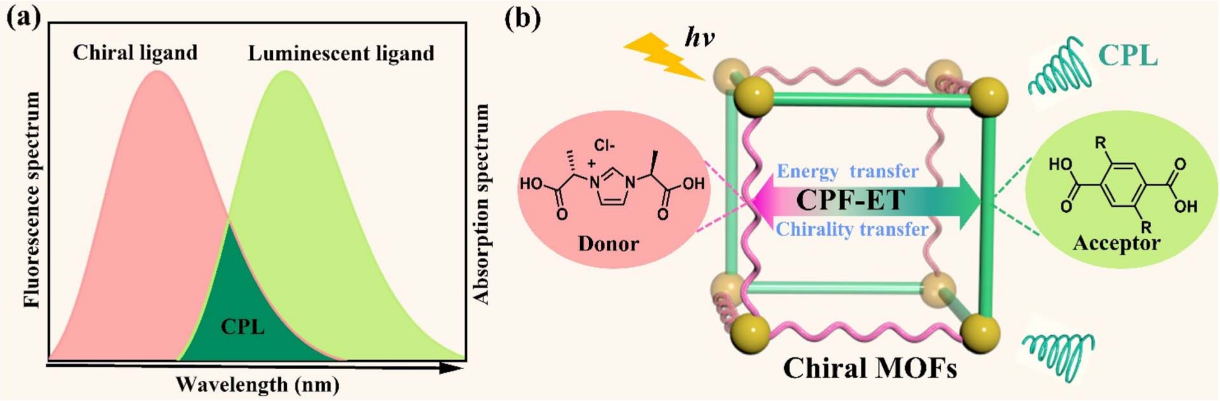

Scheme 1 (a) Schematic illustration of the CPL mechanism within CPF-ET. (b) Our design strategy of CPL-active CMOFs *via* CPF-ET.

increased further upon the introduction of functional groups such as hydroxyl or amino groups to modify the electronic properties of aromatic rings (Scheme 1b and Fig. S5–S7†). Based on these preliminary experimental results, we propose that the co-assembly of L/D-H2IDPA and TPA derivatives into a CMOF may effectively activate the CPF-ET process, resulting in outstanding CPL performance.

Building upon these considerations, we employed a dual-ligand strategy, incorporating L/D-H_2IDPA and TPA derivatives to coordinate with zinc ions, resulting in the successful synthesis of three pairs of structurally analogous CMOFs, denoted as **L/D-1**, **L/D-2**, and **L/D-3**. Optical performance evaluations demonstrated that these compounds exhibited exceptional CPL characteristics, as evidenced by $|g_{\mathrm{lum}}|$ values on the order of 10^{-1} observed in their single-crystal form. Further analysis confirmed a direct positive correlation between the magnitude of $|g_{\mathrm{lum}}|$ and the extent of spectral overlap, providing strong evidence for the scientific validity of CPF-ET as a guiding principle in the design of CPL materials. Subsequently, we experimentally confirmed their significant potential for applications in information encryption. This study not only presents a novel perspective on the design and synthesis of CPL materials but also expands the practical applicability of these advanced materials.

Results and discussion

Structural characterizations

Colorless crystals of **L-1**, with the chemical formula $Zn_2[L\text{-}IDPA]_2TPA$, were synthesized through a one-pot hydrothermal reaction, utilizing a mixture of $Zn(NO_3)_2\cdot 6H_2O$, L-H_2IDPA, and TPA in a mixed solvent system consisting of DMF, EtOH, and H_2O. Single-crystal X-ray diffraction (SXRD) analysis confirmed that **L-1** crystallizes in the orthorhombic crystal system, with the

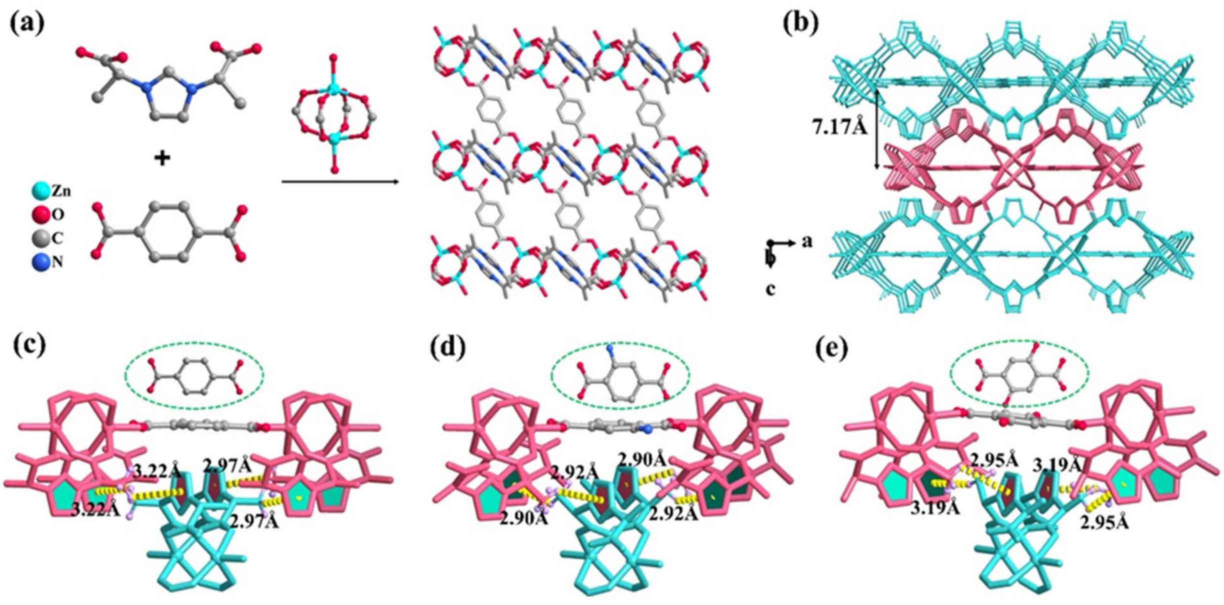

Fig. 1 (a) Diagrams illustrating the secondary building units and layer structures of **L-1**. (b) 3D stacking diagrams along the *b*-axis of **L-1**. (c)–(e) The C–H–π interaction between adjacent layers of **L-1**, **L-2**, and **L-3**.

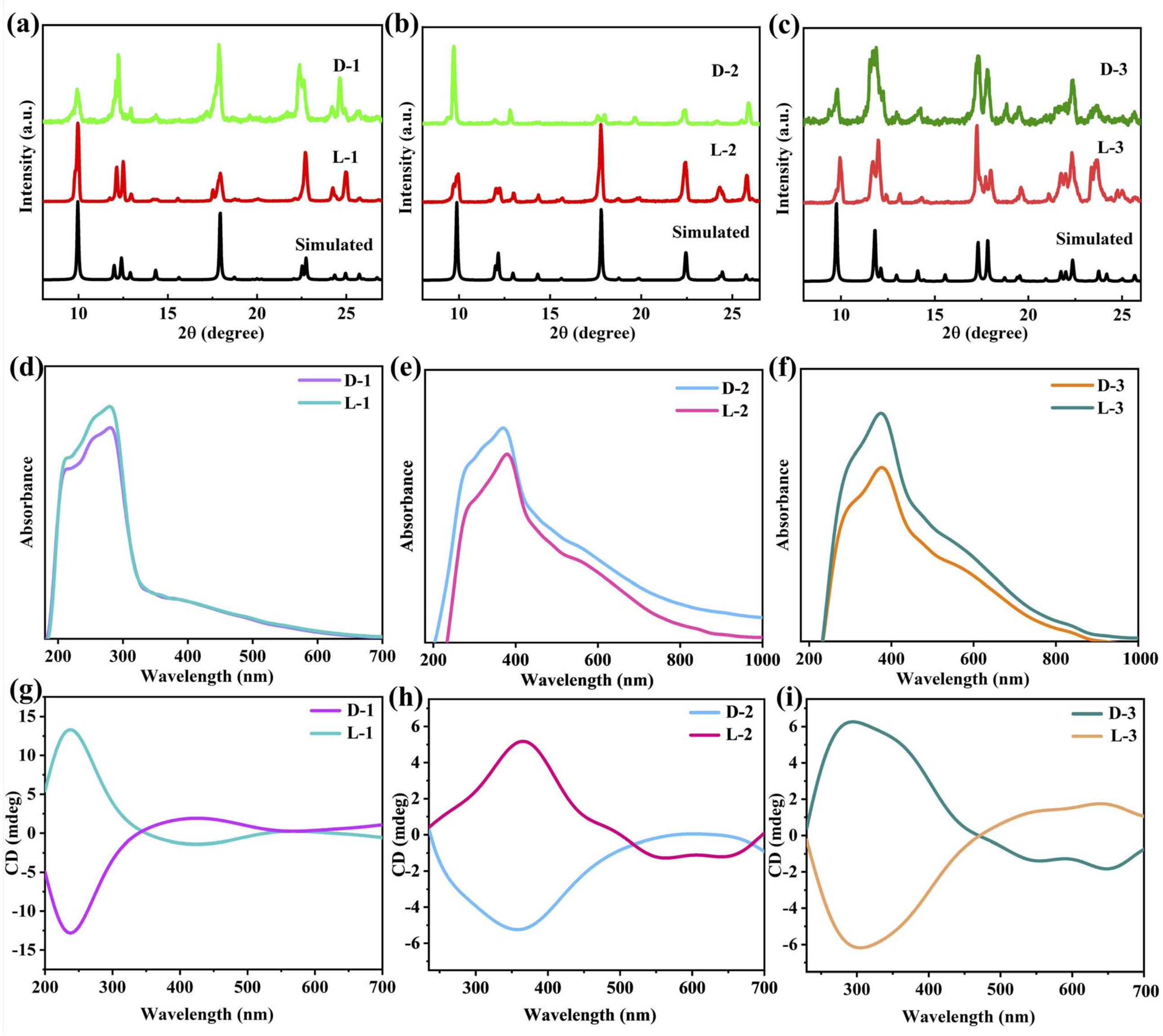

Fig. 2 Simulated and measured PXRD patterns of (a) **L/D-1**, (b) **L-/D-2**, and (c) **L/D-3**. Ultraviolet-visible absorption spectra of (d) **L/D-1**, (e) **L/D-2**, and (f) **L/D-3**. The CD spectra of (g) **L/D-1**, (h) **L/D-2**, and (i) **L/D-3**.

space group $P2_12_12_1$ (Table S1†). The binuclear zinc paddle-wheel secondary building units (SBUs) of **L-1** are constructed through coordination with two Zn(II) ions, one TPA ligand, and two IDPA ligands (Fig. S8†). A pair of IDPA ligands bridges adjacent binuclear Zn units, thereby forming double-chain structures. These one-dimensional (1D) double-chain structures further assemble into two-dimensional (2D) layered structures through the coordination of TPA ligands (Fig. 1a). These 2D layers are arranged in parallel and stacked in an …ABAB… configuration along the *b*-axis, resulting in a three-dimensional (3D) framework. Within this 3D framework, the interlayer distance between adjacent parallel layers measures 7.17 Å (Fig. 1b). Additionally, an intermolecular interaction between layers is observed, specifically a C–H–π interaction between the hydrogen atom of the methyl group in the IDPA ligand and the imidazole ring of the adjacent IDPA ligand, with distances of approximately 3.22 Å and 2.97 Å (Fig. 1c).

Under analogous reaction conditions, we successfully synthesized $[Zn_2(L\text{-}IDPA)_2(ATPA)]$ (**L-2**) and $[Zn_2(L\text{-}IDPA)_2(DHTA)]$ (**L-3**), achieved by substituting TPA with 2-amino-terephthalic acid (ATPA) and 2,5-dihydroxy-terephthalic acid (DHTA), respectively (see ESI† Experiment section). Single-crystal X-ray diffraction analysis confirmed that **L-2 and L-3** are isomorphous with **L-1**, exhibiting consistent coordination environments and bonding modes (Tables S1 and S8†). As a result, detailed descriptions of their structures are omitted here. The primary structural difference lies in the subtle change of the interlayer distance, which is induced by the additional substituents on the TPA ligand. This results in an expansion of the interlayer distance to 7.33 Å and 7.48 Å, respectively, leading to C–H–π interactions in the adjacent layers of 2.90 Å, 2.92 Å

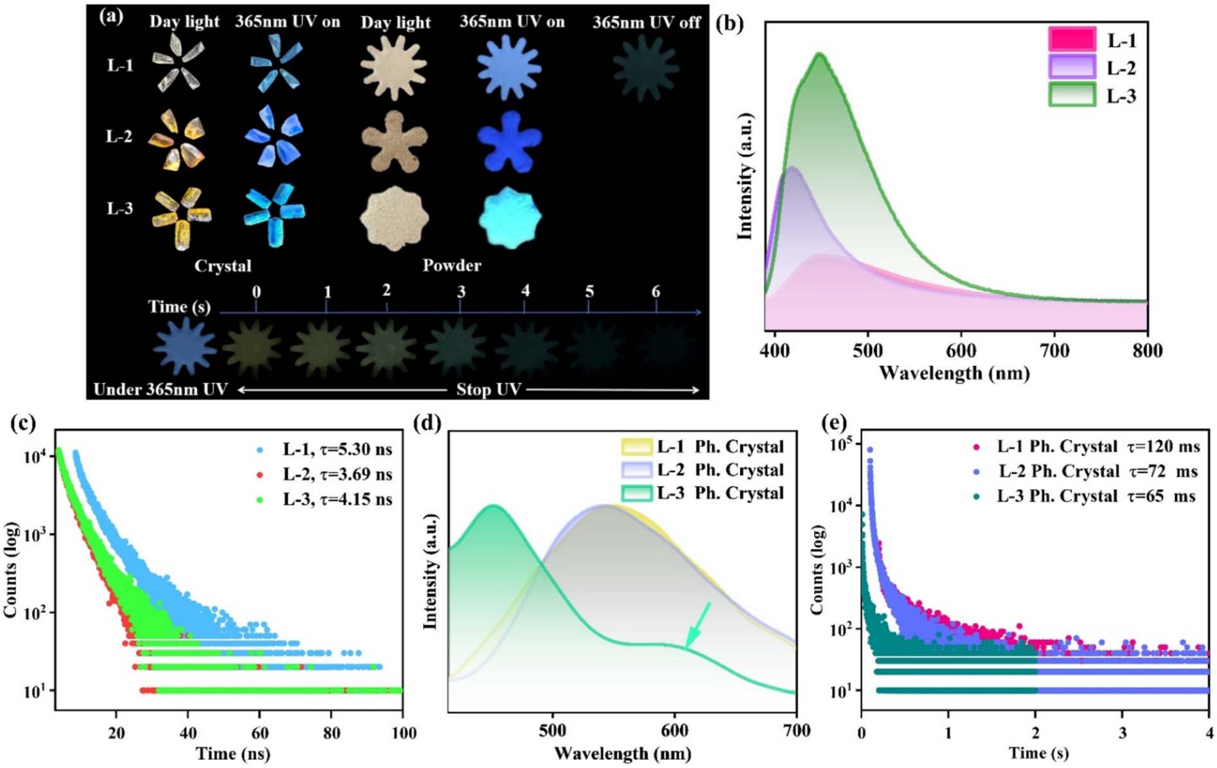

Fig. 3 (a) Images of single crystals and powders of **L-1**, **L-2**, and **L-3** in daylight, under UV irradiation at 365 nm, and **L-1** long afterglow photographs. (b) and (c) present the fluorescence spectra and fluorescence lifetimes of **L-1**, **L-2**, and **L-3**, respectively. (d) and (e) show the phosphorescence spectra and phosphorescence lifetimes of **L-1**, **L-2**, and **L-3**, respectively.

and 3.19 Å, 2.95 Å, respectively (Fig. 1d, e and S12†). Additionally, the D-enantiomers of these compounds, denoted as **D-1**, **D-2**, and **D-3**, were successfully synthesized by substituting the homochiral L-H_2IDPA with D-H_2IDPA.

Stability and light absorption properties

Powder X-ray diffraction (PXRD) analysis of the three compound pairs revealed sharp and well-defined diffraction patterns, which exhibited a high degree of congruence with the theoretical simulations, thereby unequivocally validating their exceptional crystalline quality and phase purity (Fig. 2a–c). To assess the chemical stability of these compounds, pristine samples were subjected to treatment with 11 common solvents (MeOH, EtOH, H_2O, DMF, Acetone, cyclohexane, 1,4-dioxane, dichloromethane, trichloromethane, tetrahydrofuran, Acetone) for seven days, as well as with aqueous solutions of varying pH levels (ranging from 2 to 12) for 24 hours (Fig. S15 and S16†). The PXRD patterns, which demonstrated the preservation of crystallinity, strongly indicated the remarkable chemical stability of these compounds. Additionally, thermogravimetric analysis (TGA) results confirmed the exceptional thermal stability of these complexes, which maintained their structural integrity even at elevated temperatures of approximately 335 °C (Fig. S17†). The solid-state UV-visible absorption spectra of **L-1**, **L-2**, and **L-3** display distinct absorption peaks within the wavelength range of 200–800 nm (Fig. 2d–f). Further analysis shows that the absorption peaks of **L-2** and **L-3** shift to the long wave region compared with **L-1**. The main reason is that **L-2** and **L-3** not only retain the same π–π* and n–π* transition characteristics as **L-1**, but also trigger an additional p–π* transition process when the –OH and –NH_2 substituents are incorporated into the TPA conjugate system. It is the new electron transition pathway brought about by these substituents that leads to the redshift of the absorption peak position of **L-2** and **L-3**.[33] To confirm the chirality of these CMOFs, circular dichroism (CD) spectroscopy was performed on solid-state samples prepared *via* the potassium bromide (KBr) pellet method at ambient temperature. The CD spectra of enantiomeric pairs **L/D-1**, **L/D-2**, and **L/D-3** displayed pronounced Cotton effects with mirrored signals across the 200–600 nm range, unambiguously validating their chiral characteristics and absolute configurations (Fig. 2g–i).

Photoluminescence properties

Upon air-drying, the crystals of **L-1**, **L-2**, and **L-3** exhibited consistent bulk morphologies and emitted blue, dark blue, and cyan fluorescence under UV illumination (365 nm). Remarkably, **L-1** exhibited a visible afterglow persisting for up to 6 seconds after the UV light source was extinguished (Fig. 3a). Room-temperature fluorescence measurements revealed a progressive increase in emission intensity for **L-1**, **L-2**, and **L-3** within the 400–550 nm wavelength range (Fig. 3b). This is due to the increase of electron-donating substituents (–NH_2 and –OH) on the benzene ring of the luminous ligand of the crystal, which

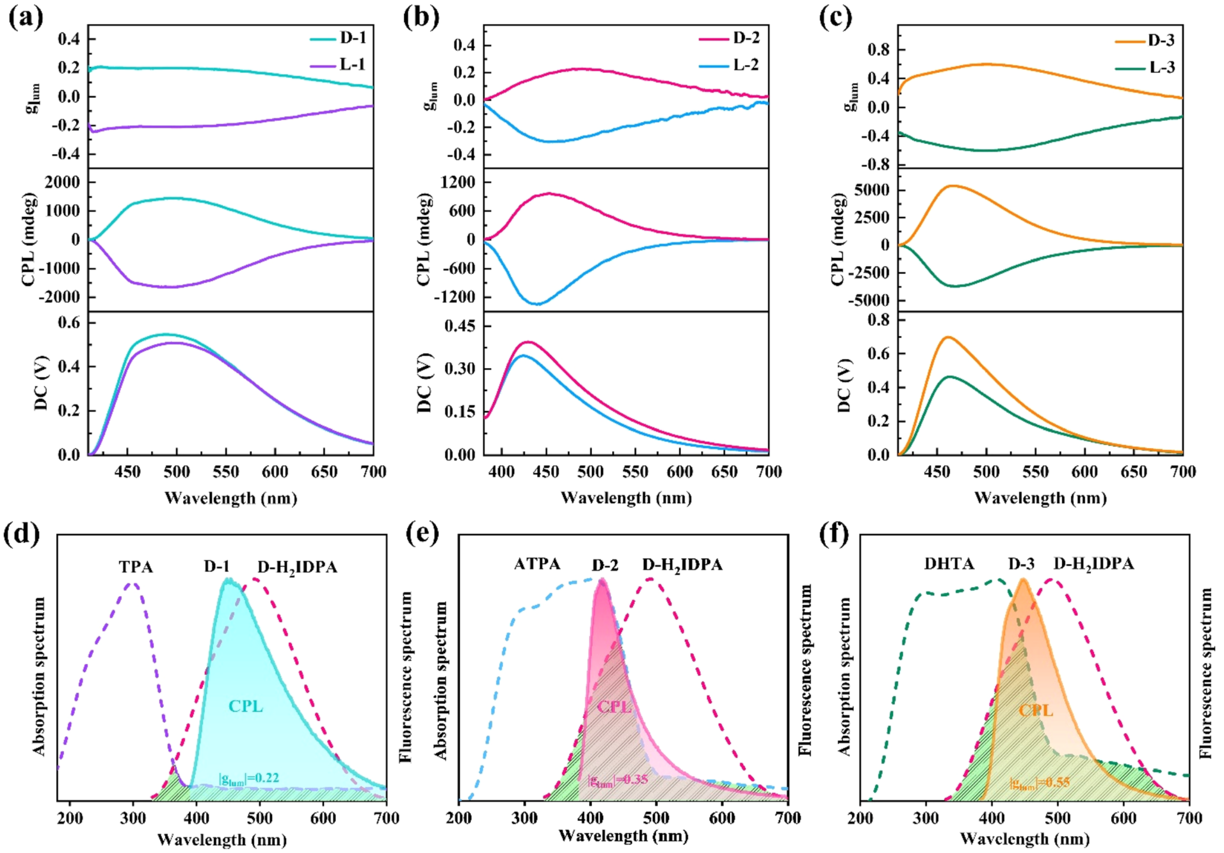

Fig. 4 CPL spectra of compounds: (a) **L/D-1**, (b) **L/D-2**, (c) **L/D-3**. Mechanism analysis with CPF-ET: (d) **D-1**, (e) **D-2**, (f) **D-3**.

enhances the conjugation effect of the MOFs structure, thus promoting the enhancement of the fluorescence intensity of the crystal. The fluorescence lifetimes of **L-1**, **L-2**, and **L-3** were determined to be 5.30 ns, 3.69 ns, and 4.15 ns, respectively (Fig. 3c). Furthermore, the fluorescence quantum yields of **L-1**, **L-2**, and **L-3** were calculated to be 6.42%, 1.76%, and 4.37%, respectively (Fig. S19–S21†). Phosphorescence testing indicates that all three crystals exhibit distinct phosphorescent emissions (Fig. 3d). Among them, **L-1** demonstrates the most pronounced phosphorescence, characterized by a lifetime of $\tau_{\mathbf{L\text{-}1}} = 120$ ms. In comparison, **L-2** and **L-3** exhibit slightly shorter lifetimes of $\tau_{\mathbf{L\text{-}2}} = 72$ ms and $\tau_{\mathbf{L\text{-}3}} = 65$ ms, respectively (Fig. 3e). The difference of crystal phosphorescence lifetime is mainly caused by the increase of the crystal layer spacing of **L-1**, **L-2**, and **L-3**, which decreases the intersystem crossing (ISC) efficiency of the crystal, and then leads to the decrease of crystal phosphorescence lifetime.

Circularly polarized luminescence performances

Subsequently, a comprehensive investigation was conducted on the CPL properties of the three pairs of enantiomeric CMOFs. To ensure data consistency and reproducibility, we systematically selected single crystals with an approximate diameter of 200 μm as test samples at room temperature and employed crystal facets oriented along the (100) direction for CPL measurements. Under the optimal excitation wavelength of 340 nm, 480 nm and 480 nm, **L/D-1**, **L/D-2**, and **L/D-3** demonstrate distinct mirror-symmetric CPL signals spanning the 400–700 nm wavelength range, with corresponding g_{lum} values of ±0.22, ±0.35, and ±0.55, respectively (Fig. 4a–c). To our knowledge, these significantly enhanced asymmetry factors position them at the forefront of reported CPL-active CMOFs (Table S3†). In addition, we utilized CPF-ET to perform a preliminary qualitative analysis of the origins and amplification of the CPL properties of these CMOFs. Through comparative analysis, we observed that the CPL signals of each D-CMOF emerge in the overlapping region of the fluorescence emission spectrum of D-H$_2$IDPA and the absorption spectrum of the corresponding TPA derivatives (Fig. 4d–f). Additionally, the magnitude of the $|g_{\text{lum}}|$ value exhibits a positive correlation with the extent of the overlapping region. These experimental results are in agreement with our previous predictions, further validating that CPL performance is directly correlated with the efficiency of CPF-ET. This finding offers robust empirical support for our research and further emphasizes the critical role of CPF-ET in guiding the synthesis of CPL-active materials.

Applications

By harnessing the highly tunable photoluminescent properties and stimulation-responsive chiral luminescence exhibited by the three enantiomeric pairs of compounds, these materials emerge as promising candidates for applications in encryption

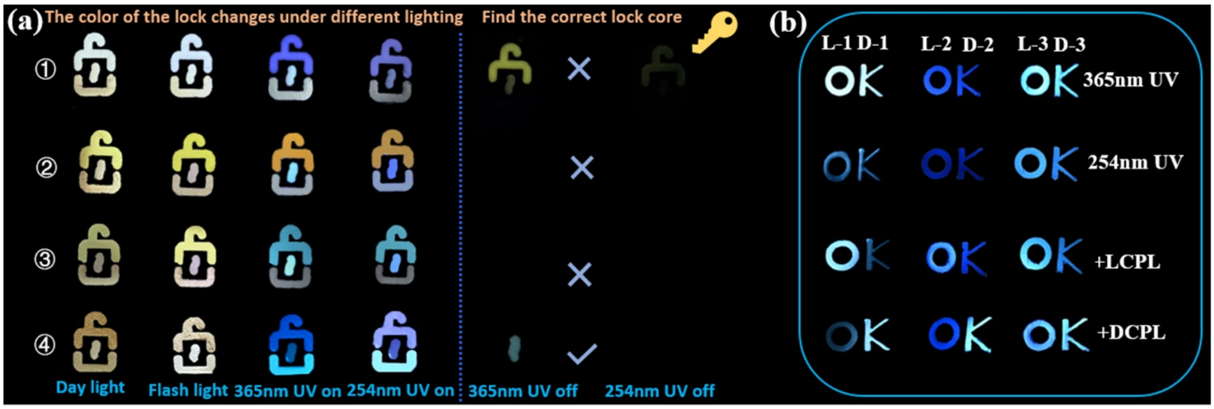

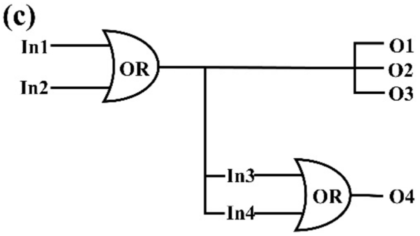

INPUT				OUTPUT			
In1 365nm	In2 254nm	In3 L-CPL	In4 R-CPL	O1 PL blue	O2 PL dark blue	O3 PL cyan	O4 CPL+=1 CPL-=0
1	0	1	0	1	0	0	1
1	0	0	1	0	0	1	0
0	1	1	0	0	1	0	1
0	1	0	1	1	0	0	0

Fig. 5 (a) Schematic diagram of application of luminescent crystals and their ligands in lock anti-counterfeiting. The picture on the left shows four different combinations of locks, with 16 color variations under different conditions. Specifically included in daylight, flashlight, 365 nm, and 254 nm UV lights. The picture on the right shows the color change of the lock after the 365 nm and 254 nm UV lights are turned off to find the correct lock that matches the key. (b) Color change of crystal patterns for **L/D-1**, **L/D-2**, and **L/D-3** under 365 nm and 254 nm UV light, and in the presence of L-CPL and D-CPL. (c) Physical electronic device with integrated chiral combinatorial logic gate. 365 nm, 254 nm, L-CPF, and D-CPF are input 1, input 2, input 3, and input 4, respectively. Blue, dark blue, cyan, and chiral luminescence intensities are defined as output 1, output 2, output 3, and output 4, respectively.

and anti-counterfeiting technologies. As shown in Fig. 5a, based on the photoluminescence properties of the crystals, four distinct "lock" patterns were generated by combining luminescent ligands (TPA, ATPA, DHTA) with the crystals (**L-1**, **L-2**, and **L-3**). The four "locks" exhibit distinct characteristics: ①–③ "lock tongues" are composed of TPA, ATPA, and DHTA, respectively, while the "lock bodies" are uniformly derived from the H_2IDPA system, and the "lock cores" originate from the **L-1**, **L-2**, and **L-3** crystal systems, respectively. The fourth "lock" is unique, as its "lock tongue", "lock body", and "lock core" are ingeniously assembled from **L-2**, **L-3**, and **L-1** crystals, respectively. Upon exposure to various light sources, these four "locks" exhibit 16 distinct color patterns, clearly demonstrating their substantial potential for multi-color anti-counterfeiting applications. In a hypothetical scenario involving a key, the long afterglow characteristics of the crystals can be utilized to match the key with its corresponding "lock". Upon irradiating these four "locks" with 365 nm and 254 nm UV lamps for several seconds, followed by turning off the lamps, it was observed that only the fourth "lock" matched the key. This methodology highlights the significant potential and broad application prospects of the long afterglow properties of crystals in the domains of information security and encryption.

Afterward, capitalizing on the remarkable CPL properties of these crystals, we investigated their potential applications in the optoelectronic domain. Initially, the L- and D-configurations of three pairs of enantiomeric crystals were organized into distinct "O" and "K" patterns, respectively. Under UV illumination at 365 nm and 254 nm, the crystals displayed pronounced and distinguishable color variations. Upon applying a left-handed circularly polarized filter (L-CPF) or a right-handed circularly polarized filter (D-CPF) over the crystal patterns, the luminescence intensities of the L- and D-type crystals exhibited varying degrees of enhancement or attenuation (Fig. 5b). Building on these observations, we designed a chiral-integrated combinational logic device (Fig. 5c). Four external stimuli were defined as inputs: input 1 (365 nm), input 2 (254 nm), input 3 (L-CPF), and input 4 (D-CPF). Inputs 0 and 1 denoted the absence and presence of stimuli, respectively. At the output level, the emission color states of the crystals were employed to encode and transmit information. Specifically, output 1 corresponded to blue, output 2 to dark blue, and output 3 to cyan. The presence or absence of these three colors states was further encoded as binary digits, 0 and 1. Output 4 leveraged variations in chiral luminescence intensity to convey information, with 0 and 1 signifying weakened and enhanced intensities, respectively. These findings highlight the potential of this crystalline material in advancing information security, data transmission, and storage technologies.

Conclusions

In conclusion, this study demonstrates the successful design and synthesis of CPL-active CMOFs using the CPF-ET mechanism. By employing a dual-ligand strategy, three pairs of CMOFs (**L**/**D-1**, **L**/**D-2**, and **L**/**D-3**) were synthesized, achieving excellent photoluminescence characteristics and exceptional $|g_{\mathrm{lum}}|$ values up to 0.55. A strong correlation between CPF-ET efficiency and CPL performance was established, providing valuable insights for the rational design of chiral luminescent materials. The outstanding CPL properties of these CMOFs enabled their application in chiral combinational logic devices, highlighting their potential for information encryption and optoelectronic technologies. This work not only advances the understanding of CPL mechanisms but also paves the way for the practical integration of CMOFs into advanced optical systems.

Data availability

The data supporting this article have been included as part of the ESI.† Crystallographic data for **D**/**L-1**, **D**/**L-2** and **D**/**L-3** has been deposited at the Cambridge Crystallographic Data Centre (CCDC) under [2415207–2415212] and can be obtained from http://www.ccdc.cam.ac.uk/structures/.

Author contributions

H. Zheng performed the experiments and analysis, and was specifically responsible for survey conceptualization, data management, formal analysis, research methods, manuscript writing, review and editing. Q. Wang was responsible for the supervision and help. F. Wang participated in the guidance of the structure diagram. S. Li participated in conception, funding, resources, supervision, validation, manuscript writing, review and editing. J. Zhang participated in funding acquisition, supervision and verification.

Conflicts of interest

There are no conflicts to declare.

Acknowledgements

This work was supported by National Key Research & Development Program of China [2022YFA1503300] and National Natural Science Foundation of China [22471273].

Notes and references

1 N. Mavragani, D. A. Gálico, A. A. Kitos and M. Murugesu, Near-Infrared Magnetic Circularly Polarized Luminescence and Slow Magnetic Relaxation in a Tetrazinyl-Bridged Erbium Metallocene, *J. Am. Chem. Soc.*, 2025, **147**, 1387–1391.

2 O. Oki, C. Kulkarni, H. Yamagishi, S. C. J. Meskers, Z.-H. Lin, J.-S. Huang, E. W. Meijer and Y. Yamamoto, Robust Angular Anisotropy of Circularly Polarized Luminescence from a Single Twisted-Bipolar Polymeric Microsphere, *J. Am. Chem. Soc.*, 2021, **143**, 8772–8779.

3 D. F. Caffrey, T. Gorai, B. Rawson, M. Martínez-Calvo, J. A. Kitchen, N. S. Murray, O. Kotova, S. Comby, R. D. Peacock, P. Stachelek, R. Pal and T. Gunnlaugsson, Ligand Chirality Transfer from Solution State to the Crystalline Self-Assemblies in Circularly Polarized Luminescence (CPL) Active Lanthanide Systems, *Adv. Sci.*, 2024, **11**, 2307448.

4 M. Kazem-Rostami, A. Orte, A. M. Ortuño, A. H. G. David, I. Roy, D. Miguel, A. Garci, C. M. Cruz, C. L. Stern, J. M. Cuerva and J. F. Stoddart, Helically Chiral Hybrid Cyclodextrin Metal–Organic Framework Exhibiting Circularly Polarized Luminescence, *J. Am. Chem. Soc.*, 2022, **144**, 9380–9389.

5 W. R. Kitzmann, J. Freudenthal, A. P. M. Reponen, Z. A. VanOrman and S. Feldmann, Fundamentals, Advances, and Artifacts in Circularly Polarized Luminescence (CPL) Spectroscopy, *Adv. Mater.*, 2023, **35**, 2302279.

6 G. Longhi, E. Castiglioni, J. Koshoubu, G. Mazzeo and S. Abbate, Circularly Polarized Luminescence: A Review of Experimental and Theoretical Aspects, *Chirality*, 2016, **28**, 696–707.

7 J. Kumar and T. Nakashima, Amplifying circularly polarized luminescence in chirality-matched dye-silver clusters, *Chem*, 2024, **10**, 1628–1630.

8 W. Cao, Y. Tang, Y. Cui and G. Qian, Energy Transfer in Metal–Organic Frameworks and Its Applications, *Small. Struct.*, 2020, **1**, 2000019.

9 Y. Wu, C. Yan, X. S. Li, L. H. You, Z. Q. Yu, X. Wu, Z. Zheng, G. Liu, Z. Guo, H. Tian and W. H. Zhu, Circularly Polarized Fluorescence Resonance Energy Transfer (C-FRET) for Efficient Chirality Transmission within an Intermolecular System, *Angew. Chem., Int. Ed.*, 2021, **60**, 24549–24557.

10 K. Yang, S. Ma, Y. Wu, B. Zhao and J. Deng, Circularly Polarized Fluorescence Energy Transfer for Constructing Multicolor Circularly Polarized Luminescence Films with Controllable Handedness, *Chem. Mater.*, 2023, **35**, 1273–1282.

11 X. Yang, X. Gao, Y.-X. Zheng, H. Kuang, C.-F. Chen, M. Liu, P. Duan and Z. Tang, Recent Progress of Circularly Polarized Luminescence Materials from Chinese Perspectives, *CCS Chem.*, 2023, **5**, 2760–2789.

12 E. A. Dolgopolova, D. E. Williams, A. B. Greytak, A. M. Rice, M. D. Smith, J. A. Krause and N. B. Shustova, A Bio-inspired Approach for Chromophore Communication: Ligand-to-Ligand and Host-to-Guest Energy Transfer in Hybrid Crystalline Scaffolds, *Angew. Chem., Int. Ed.*, 2015, **54**, 13639–13643.

13 Y.-X. Yuan, J.-H. Jia, Y.-P. Song, F.-Y. Ye, Y.-S. Zheng and S.-Q. Zang, Fluorescent TPE Macrocycle Relayed Light-Harvesting System for Bright Customized-Color Circularly Polarized Luminescence, *J. Am. Chem. Soc.*, 2022, **144**, 5389–5399.

14 J. Y. Wang, Y. Si, X. M. Luo, Z. Y. Wang, X. Y. Dong, P. Luo, C. Zhang, C. Duan and S. Q. Zang, Stepwise Amplification of Circularly Polarized Luminescence in Chiral Metal Cluster Ensembles, *Adv. Sci.*, 2023, **10**, 2207660.

15 S. Yang, S. Zhang, F. Hu, J. Han and F. Li, Circularly polarized luminescence polymers: From design to applications, *Coord. Chem. Rev.*, 2023, **485**, 215116.

16 K. Yang, R. Zhang, Y. Liu, B. Zhao, Y. Wu and J. Deng, Circularly Polarized Phosphorescence Energy Transfer Combined with Chirality-Selective Absorption for Modulating Full-Color and White Circularly Polarized Long Afterglow, *Angew. Chem., Int. Ed.*, 2024, **63**, e202409514.

17 Y. Wu, C. Yan, X. S. Li, L. H. You, Z. Q. Yu, X. Wu, Z. Zheng, G. Liu, Z. Guo, H. Tian and W. H. Zhu, Circularly Polarized Fluorescence Resonance Energy Transfer (C-FRET) for Efficient Chirality Transmission within an Intermolecular System, *Angew. Chem., Int. Ed.*, 2021, **60**, 24549–24557.

18 D. Yang, P. Duan, L. Zhang and M. Liu, Chirality and energy transfer amplified circularly polarized luminescence in composite nanohelix, *Nat. Commun.*, 2017, **8**, 15727.

19 N. R. Catarineu, A. Schoedel, P. Urban, M. B. Morla, C. A. Trickett and O. M. Yaghi, Two Principles of Reticular Chemistry Uncovered in a Metal–Organic Framework of Heterotritopic Linkers and Infinite Secondary Building Units, *J. Am. Chem. Soc.*, 2016, **138**, 10826–10829.

20 J. Robin, N. Audebrand, C. Poriel, J. Canivet, G. Calvez, T. Roisnel, V. Dorcet and P. Roussel, A series of chiral metal–organic frameworks based on fluorene di- and *tetra*-carboxylates: syntheses, crystal structures and luminescence properties, *CrystEngComm*, 2017, **19**, 2042–2056.

21 Z. Wei, Z.-Y. Gu, R. K. Arvapally, Y.-P. Chen, R. N. McDougald, J. F. Ivy, A. A. Yakovenko, D. Feng, M. A. Omary and H.-C. Zhou, Rigidifying Fluorescent Linkers by Metal–Organic Framework Formation for Fluorescence Blue Shift and Quantum Yield Enhancement, *J. Am. Chem. Soc.*, 2014, **136**, 8269–8276.

22 U. Huizi-Rayo, X. Gastearena, A. M. Ortuño, J. M. Cuerva, A. Rodríguez-Diéguez, J. A. García, J. Ugalde, J. M. Seco, E. S. Sebastian and J. Cepeda, Influence of Tartrate Ligand Coordination over Luminescence Properties of Chiral Lanthanide-Based Metal–Organic Frameworks, *Nanomaterials*, 2022, **12**, 3999.

23 S. Lee, E. A. Kapustin and O. M. Yaghi, Coordinative alignment of molecules in chiral metal–organic frameworks, *Science*, 2017, **353**, 794.

24 H. R. Fu, N. Wang, X. X. Wu, F. F. Li, Y. Zhao, L. F. Ma and M. Du, Circularly Polarized Room-Temperature Phosphorescence and Encapsulation Engineering for MOF-Based Fluorescent/Phosphorescent White Light-Emitting Devices, *Adv. Opt. Mater.*, 2020, **8**, 2000330.

25 W. Shang, X. Zhu, T. Liang, C. Du, L. Hu, T. Li and M. Liu, Chiral Reticular Self-Assembly of Achiral AIEgen into Optically Pure Metal–Organic Frameworks (MOFs) with Dual Mechano-Switchable Circularly Polarized Luminescence, *Angew. Chem., Int. Ed.*, 2020, **59**, 12811–12816.

26 Z. Sharifzadeh, K. Berijani and A. Morsali, Chiral metal–organic frameworks based on asymmetric synthetic strategies and applications, *Coord. Chem. Rev.*, 2021, **445**, 214083.

27 A. H. Alawadhi, S. Chheda, G. D. Stroscio, Z. Rong, D. Kurandina, H. L. Nguyen, N. Rampal, Z. Zheng, L. Gagliardi and O. M. Yaghi, Harvesting Water from Air with High-Capacity, Stable Furan-Based Metal–Organic Frameworks, *J. Am. Chem. Soc.*, 2024, **146**, 2160–2166.

28 X. Wang, Z. Wang, Z. Wang, T.-F. Liu, S. Li, F. Wang and J. Zhang, Synthesis of Homochiral N-Heterocyclic Carbene-Based Nanosheets for Enhanced Asymmetric Catalysis, *Adv. Sci.*, 2024, **12**, 2412592.

29 H. R. Zheng, Q. Q. Wang, X. C. Wang, F. Wang, S. Li and J. Zhang, Dual-ligand chiral MOFs exhibiting circularly polarized room temperature phosphorescence for anti-counterfeiting, *Sci. China. Chem.*, 2025, **68**, 1–7.

30 X.-B. Yin, Y.-Q. Sun, H. Yu, Y. Cheng and C. Wen, Design and Multiple Applications of Mixed–Ligand Metal–Organic Frameworks with Dual Emission, *Anal. Chem.*, 2022, **94**, 4938–4947.

31 X. Yang and D. Yan, Strongly Enhanced Long-Lived Persistent Room Temperature Phosphorescence Based on the Formation of Metal–Organic Hybrids, *Adv. Opt. Mater.*, 2016, **4**, 897–905.

32 J. Yuan, J. Dong, S. Lei and W. Hu, Long afterglow MOFs: a frontier study on synthesis and applications, *Mater. Chem. Front.*, 2021, **5**, 6824–6849.

33 Y. Li, T. Gai, Y. Lin, W. Zhang, K. Li, Y. Liu, Y. Duan, B. Li, J. Ding and J. Li, Eight Cd(II) coordination polymers with persistent room-temperature phosphorescence: intriguing dual emission and time-resolved afterglow modulation, *Inorg. Chem. Front.*, 2020, **7**, 777–785.